JPPIPA 9(1) (2023)

Jurnal Penelitian Pendidikan IPA

Journal of Research in Science Education

http://jppipa.unram.ac.id/index.php/jppipa/index

Horizontal to Vertical Spectral Ratio (HVSR) Analysis of the Passive Seismic Data on Alluvial Lithology: An Example from Bandung Basin Rim

Evi Fazriati[1,2], Muhammad Randy Azhari[1], Abdul Hakam[3], Widya Utama[4], Yudi Rosandi[1*]

[1] Department of Geophysics, University of Padjadjaran, Sumedang Indonesia.
[2] Postgraduate Physics Study Program, University of Padjadjaran, Sumedang, Indonesia.
[3] Department of Civil Engineering, University of Andalas, Indonesia.
[4] Department of Geophysics Engineering, Institut Teknologi Sepuluh Nopember, Indonesia.

Received: December 15, 2022
Revised: January 26, 2023
Accepted: January 28, 2023
Published: January 31, 2023

Corresponding Author:
Yudi Rosandi
rosandi@geophys.unpad.ac.id

DOI: 10.29303/jppipa.v9i1.2962

Abstract: Bandung basin is surrounded by active volcanoes at the center of Western Java region. Soil type of this area consists mostly of volcanic alluvial, formed by the past volcanic activities. At this location, we performed passive seismic surveys to reveal the sedimentary characteristics using a triaxial seismometer, to study the properties which have potential implications on environmental aspects, such as natural disaster mitigation and the city planning. In this work we reported the analysis of three component vibration signals by means of the Horizontal to Vertical Spectral Ratio (HVSR) calculation to identify the sediment thickness through the dominant frequency of the earth vibration. The method signal processing successfully revealed the amplification factor of the area, which is very important to determine the potential ground motion induced disasters. The data was collected using a laboratory developed seismic logging device with sensitivity of 0.28 ± 5% V·s/cm. The signal preconditioning was carried out to shape the acquired signals with high noise level, prior to the HVSR calculation. From the measurements and computation, we obtained the thickness variation at the chosen survey area of around 32 to 64 meters, corresponding to the measured dominant frequency of around 2.5 to 5.0 Hz. The results agree very well with the reference sediment thickness measured by the microtremor surveys. The vibration frequencies are also consistent with the range suggested by the literature.

Keywords: HVSR; Microtremor; Signal processing

Introduction

The passive seismic method records background vibrations of the earth originated from ambient noise. The method is non-destructive and robust to identify the sedimentary layer properties through the mechanical vibration. The resonance of the ground, which is related directly to the mechanical properties of the medium, amplifies a specific frequency range which reflects the geometrical situation of the measurement site. As long as the properties are known, geophysicists can derive the thickness of the medium, considering a semi-infinite lateral geometry, from the resonance frequency. However, due to a high noise level and the complexity of ambient vibration, the frequency cannot be directly observed from the recorded signals, having low frequencies in the order of 1 Hz (Bonnefoy-Claudet et al., 2009; Landés et al., 2010; Rezaei et al., 2017). Hence, an advanced signal processing procedure is required prior to the signal interpretations. The method is commonly recognized as a microtremor method when the measured ground vibration amplitude is in range of 0.1-1 μm, corresponding to the amplitude velocity of 0.001-0.01 cm/s (Mirzaoglu et al., 2003). The method can be effectively used to identify the sedimentary conditions, which can be derived to obtain the vulnerability of an area to vibrations induced by events such as earthquakes. The elastic property of the lithosphere

How to Cite:
Fazriati, E., Azhari, M.R., Hakam, A., Utama, W., & Rosandi, Y. (2023). Horizontal to Vertical Spectral Ratio (HVSR) Analysis of the Passive Seismic Data on Alluvial Lithology: An Example from Bandung Basin Rim. *Jurnal Penelitian Pendidikan IPA*, *9*(1), 402–411. https://doi.org/10.29303/jppipa.v9i1.2962

allows the amplification and reduction of the incoming mechanical wave, which are characterized by the parameters, such as wave velocity, the elastic moduli of the medium, and the geometrical condition (sedimentary thickness) of the area.

In general, microtremor recording requires three-component seismometer consisting of two horizontal components (east-west, north-south), and a vertical component (up-down). The data analysis is performed using the Horizontal to Vertical Spectral Ratio (HVSR) method. The principle of this method is the estimation of the spectrum ratio of the horizontal to the vertical components. The HVSR curve shows the value of the amplification factor and dominant frequency that can represent the sedimentary conditions and geometry (Herak, 2008). The dominant frequency value is inversely related to the thickness of the sediment layer on the surface (Bao et al., 2019). The thicker the sediment layer in an area, the smaller the measured frequency (Kanai, 1983). The amplification factor, which is exponentially related to the sediment thickness, is a measure of the susceptibility of the soil to ground motion (Bowden et al., 2017). The value reflects the sensitivity of an area when exposed to shock events (Kaiser et al., 2014).

The HVSR calculation has an advantage that it can determine the frequency directly without having an a priori knowledge of the geological conditions of the sub-surface. The method was introduced by Nogoshi et al. (1971) and extensively revised by Nakamura (1989), has been used in numerous studies for estimating local seismic ground response, particularly in Slovenia, Italy, and Croatia (Di Giacomo et al., 2005; Gosar, 2007; Stanko et al., 2017). HVSR is very robust, in the sense that it requires only three component measurements of vibration to reveal an accurate determination of the natural or fundamental soil frequency. The sites' resonance frequency and peak amplitude can be obtained without any high energy sources, both naturally occurring (earthquake activities) and man-made ones (Imposa et al., 2018).

The method is very useful to be applied in disaster mitigation related to ground vibration such as landslide, earthquake identification, and building stability (Kagawa et al., 2017; Suhendra et al., 2018). In addition, one of the important uses of the microtremor method is to be able to determine the characteristics of sediment thickness in an area that is widely used for microzonation landslides occurrence potency (Gosar, 2017; Marjiyono, 2010). Microtremor measurements accompanied by HVSR calculation have been carried out in several locations with different geological conditions and exposed many important information of the sub surface. Measurements in the karst area have been carried out to determine the thickness of the surface sediment. The dominant frequency value obtained in the Karst area is relatively high > 10 Hz (Chemsitra et al., 2018), due to the hardness of the subsurface medium and the thin sedimentary layer. In the alluvial basin area, a high seismic wave amplification factor (up to a factor of 20) was found with the dominant frequency ranging around 0.5 to 5 Hz (Bindi et al., 2011).

In this work we presented the analysis of three component vibration signals to identify the sediment thickness via the dominant frequency of the vibration, which was carried out using direct measurement data performed at an area located at the Bandung Basin rim. The method has successfully revealed the amplification factor of the area, which is very important to determine the potential ground motion induced disasters. The aim is to verify the functionality of a system of a low-cost microtremor apparatus along with the developed microtremor processing algorithm. The development of the system will be useful to perform environmental monitoring related to the geological disaster mitigation, as well as the microzonation of a local area to be used in building a resilient infrastructure.

Method

The data acquisition was carried out in two locations with a contrast geomorphological condition. The first area is on a plateau of thick sediment (labeled by **A**) and the second area is in a valley region (labeled by **B)**. The second area is located along a water flow path, specifically chosen so that the sediment is eroded and thin. The duration of data collection at each point is 10 minutes. During the data acquisition, we avoided noises that potentially can be caused by the surrounding environmental activities. The acquisition was carried out using a triaxial seismometer developed in the laboratory, namely the SeismoLog instrument (Figure 1), with analog to digital conversion resolution of 10 bits and the voltage gain of 200 times in a differential measurement mode. The range of the voltage measurement is $\pm 10^{-5}$ volt. The seismometer is of type ST-4.5N triaxial geophone with natural frequency of 4.5±10% and sensitivity of 28.8±5% V·s/cm. The seismometer consists of two horizontal components (east-west and north-south) and one vertical component (up-down). To ease the processing work, we store the data in JSON file formats, consisting of several measurement parameters including the duration of data in seconds, the data number, and the three-component signal data.

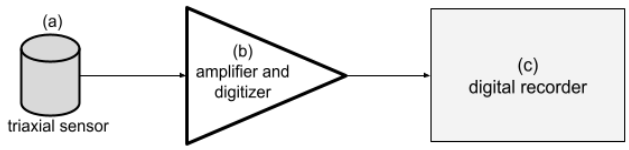

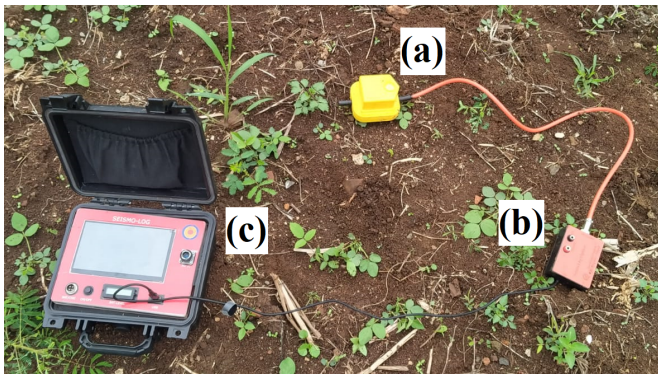

Figure 1. The SeismoLog instrument used in the data acquisition process. (a) a three-component seismometer sensor, (b) digitizer device to convert ground vibration data into digital form, (c) the main unit used to store and display the measurement data results

In the measurement, the signal is acquired alongside with the environmental noises. Noises originated from specific events create spikes in the signal, whereas the ones originating from ambient sources are composed in the recorded data. Hence, a preconditioning data processing is necessary to achieve a correct interpretation. Data preconditioning is done by reducing or removing outlier data by doing selection of the recorded data. In this work we removed the noisy data indicated by the presence of spikes.

To remove noises composed in the data, we perform filtering and windowing procedures. To remove frequencies outside the intended spectrum, we apply the Butterworth band-pass filter, with the low-cut and high-cut frequencies of 2 Hz and 10 Hz, respectively. The frequencies outside this spectrum are considered as noise. To handle the artefact due to a definite sampling period, we use the Hamming window. After these preprocessing procedures, the data is transformed into the frequency domain using a standard Fast Fourier Transform. The transformation allows the spectral analysis of the signal. However, due to the fluctuation in the frequency domain, a smoothing procedure is required to determine the peaks inside the spectrum. The peaks identify the dominant frequencies, in which the medium is vibrating. We assume the resonance frequency as the highest peak. To smoothen the spectrum, we utilized the second order low-pass Butterworth filter. This time, the filter is not used to remove unwanted frequency, but merely to remove fast fluctuations of frequencies.

The determination of the dominant frequency is done by calculating the horizontal to vertical ratio, H, using the following equation:

$$H = \frac{\sqrt{X^2 + Y^2}}{Z} \tag{1}$$

Where X, Y, and Z denote the east-west, north-south, and vertical spectrum components, respectively. We take the spectral magnitude after the smoothing procedure to perform the calculation. The peaks of the curve show dominant frequencies, whereas the maximum peak is the resonance which is used to calculate the thickness of the sediment layer. We may approximate the resonance frequency in a trivial way as follows. Consider a medium having a semi-infinite lateral dimension, which is freely moving in the vertical direction. Using Hooke's law for the vibration of an elastic medium, we may connect the geometry of the medium to the resonance vibration mode via the Young's modulus. Taking the vertical stiffness of the medium as,

$$k = \frac{E}{h}\Omega \tag{2}$$

Where, E is the modulus and Ω is an area on the topsoil. In this case h represents the height, hence the thickness of the medium. For many seismological problems, it is sufficient to take the first Lame parameter (λ) equal to the shear modulus and the Poisson ratio of v=0.25. In this situation E is related to the shear velocity (v_s) as,

$$E = 5\rho v_s^2/2 \tag{3}$$

with, ρ is the mass density. Taking the resonance frequency as,

$$f_0 = \frac{1}{2\pi}\sqrt{\frac{k}{\rho \cdot \Omega \cdot h}} \tag{4}$$

The thickness can be obtained using the following relation,

$$f_0 = 0.25\frac{v_s}{h} \tag{5}$$

In this work, we took v_s=640 m/s based on the previous measurements at the same location, by the Center for Geological Survey, Indonesia (PSG) (Telford, 2021). We define the resonance frequency as the most dominant peak, i.e. the highest, in the spectrum curve. To determine the amplification factor value, A, which represents the vulnerability of potential disasters due to ground motion, we use following the equation:

$$A = \frac{\rho_b v_{sb}}{\rho_s v_{ss}} \exp\left(-\frac{\pi f_0 h}{Q_s v_{ss}}\right) \tag{6}$$

Thickness, and Q_s denotes the quality factor of surface sedimentary rock layers. Table 1 shows the range of parameters used in the calculation. The actual value which is substituted into eq. 6 depends on the

measurement coordinates. For this purpose, we refer to the map in literature (Telford, 2021).

Table 1. The Range of Parameters Used to Calculate the Amplification Factor According to Literature (Dvorkin et al., 2006; Telford et al., 1990)

Parameter	Value
ρ_s	1.92 gr/cm³
ρ_b	1.98 gr/cm³
v_{ss}	120-195 m/s
v_{sb}	520-880 m/s
Q_s	5-10

To obtain a certainty of the amplitude spectral value the segmented spectral average was taken. We calculated the standard deviation to determine the level of fluctuation of the frequency inside the segment of 1 Hz width. Using this method, we are able to define the standard error of the obtained value. For each segment the average ($\bar{X}$), standard deviation (σ) and standard error (ε), is calculated by,

$$\bar{X} = \frac{1}{M}\sum_{i=0}^{N} X_i \quad (7)$$

$$\sigma = \sqrt{\frac{\sum_{i=0}^{N}(X_i - \bar{X})^2}{n-1}} \quad (8)$$

$$\varepsilon = \frac{\sigma}{\sqrt{n}} \quad (9)$$

where M is the segment width and N is the number of total data points.

Result and Discussion

The exemplary three-component microtremor signal is shown in Figure 2. The sample time of the measurement of the data is 10 minutes, with the obtained number of datum of 321122. Thus, the sample rate (f_s) of the acquisition is 535 data/s. The data acquisition did not only record the ambient signal vibration, but also the noise. This can be indicated by the presence of spikes in the signal. This type of noise was eliminated by removing data containing spikes. The removal was done consistently to all the components, i.e. at the exact same time. Figure 2 shows the original data, pointing out the containing spike noise. The amplitude is the measured vibration velocity expressed in the measured voltage (in volts) of the analog to digital converter device. However, for the sake of simplicity we use an arbitrary unit in the y-axis. Short impulses with amplitude more than a defined threshold value are considered noise spikes, hence any parts of the signal containing such spikes are removed. In our case the threshold value is 1 millivolt, which may vary according to the instrumentation system specification. The processing was then carried out to the remaining signal, as long as the sampling criterion is met, that is, a segment of signal must accommodate the range of intended frequency according to the Nyquist condition (Shi et al., 2018)

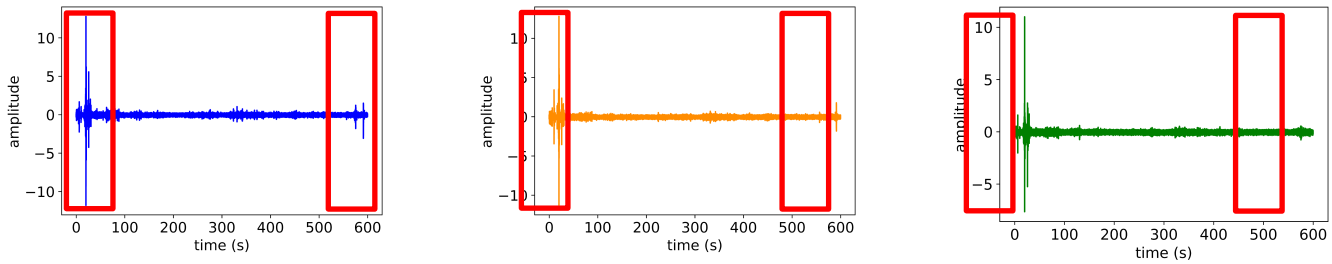

Figure 2. Example of signal data recording at measurement location A4, taken in a ten-minute sample periode. The x-axis indicates sample time, and y-axis indicates amplitude in arbitrary scale. Inside the red square are data containing spike noise which are eliminated. (Blue) East-West horizontal; (yellow) North-South horizontal, and (green) vertical up-down

The signal preprocessing procedure is applied only to the remaining data, consisting of only the ambient vibration signals. The filtering stage was performed to remove unwanted frequencies and also smoothen the discrete signal inside the spectrum under consideration, followed by the application of the chosen window function which is necessary to reduce the discontinuity effect at the edges of the signal induced by the finite sample time. Figure 3 shows the shape of the signal after applying these procedures. Since the resolution of our 10 bits ADC device is not very high, the range of digital measurement is from -511 to 512, the digital error cannot be avoided. Thus, the filtering routine was not only to remove the frequency range outside the intended spectrum, but also smoothen the zaggy nature of the acquired digital signal. These preprocessing steps have a large effect on the Fourier transformation, so that the signal in the frequency domain is easier to analyze.

The acquired signal is the superposition of all ranges of possible frequencies. In this case, the signal is

the composition of coherent vibration modes in the quasi-continuous range inside the bandwidth of 8 Hz. According to the resonance, which is dependent on the geometrical situation of the measurement site, some vibrations are attenuated, and some appear to be more dominant. In order to observe qualitatively the dominant frequencies, we applied a smoothing procedure using the Butterworth filter of the second order. Note that this procedure was carried out simply to remove fluctuation and exhibit the collective frequency profile, hence ease the identification of the modes.

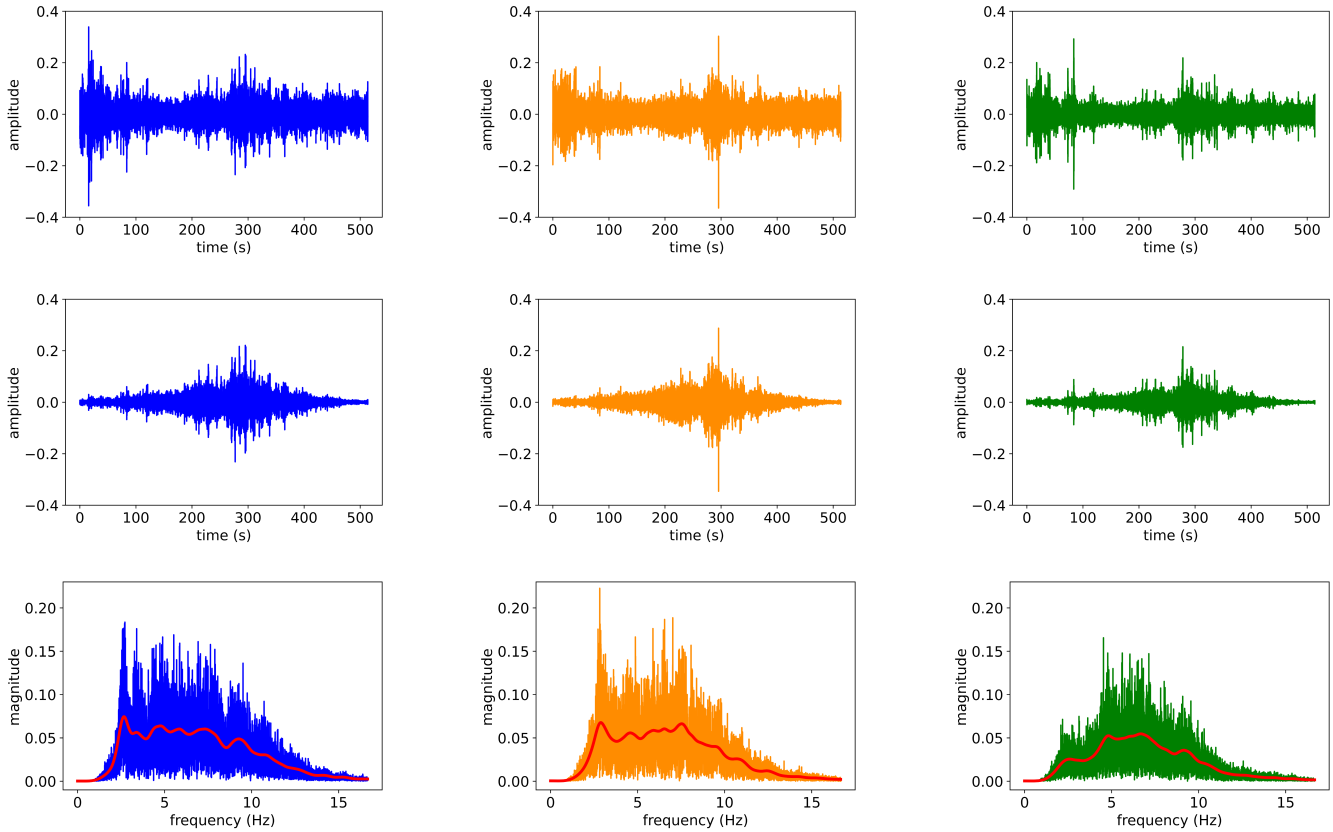

Figure 3. An exemplary plot of signal after applying the filtering procedure, left to right (upper), after applying Hamming window (middle), and the frequency domain, blue is the East-West, orange is the North-South, and green is the vertical component. Red line shows the curve after the smoothing procedure

The resonance frequency of the measurement site was identified via the HVSR calculation based on eq. 1, which is applied to the magnitude of the spectrum after the smoothing procedure, i.e. the lines shown in red, in the spectrum plot of figure 3. We show some exemplary data in figure 5 and 6. It is expected that the peak at site A ranges in lower frequencies compared to those of site B. This is consistent with the geological condition of the sites, where A is located in a thick sedimentation and B in a shallow sedimentation area. The frequency domain plot in figure 3, demonstrates a larger area under the lateral spectrum curve and showed a definite peak at low frequency of around 2.5 Hz. This indicates that the ground is vibrating more freely in the lateral than the vertical direction. We presume that the low frequency peak indicates the vast area of the plateau. In comparison, figure 4 shows the frequency plot of an exemplary data at location B. As expected, the vibration frequency is higher compared to A, and the peaks in the lateral direction are higher in frequency and smaller in magnitude. This fact demonstrates that the site is confined geometrically in a small area by its surroundings, even though the lateral vibration dominates. To discuss the phenomenon more quantitatively, we took the weight of the magnitude spectral profile, $M(f)$, as the area under the curve, as follows,

$$W = \int_{-\infty}^{\infty} M(f)df \tag{10}$$

A large value of W indicates the large vibration amplitude. From the calculation we obtained, for location A the lateral amplitude is 1.4 times the vertical vibration. For location B, it is 1.2 times the vertical vibration. The lateral vibration in A is almost twice of amplitude compared to location B.

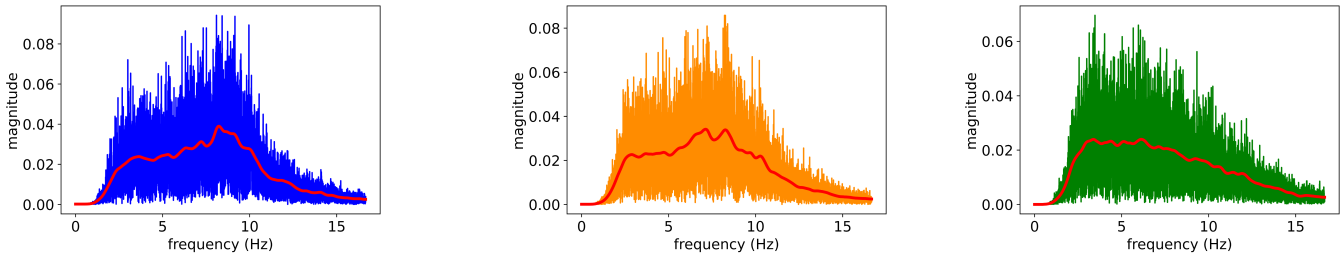

Figure 4. An exemplary plot of signal in the frequency domain from site B, blue is the East-West, orange is the North-South, and green is the vertical component. Red line shows the curve after the smoothing procedure

The HVSR calculation successfully emphasizes the resonance frequency, as shown in figure 5 and 6. We put a list of calculated frequencies in table 2 and table 3. Our instrument and processing algorithm was able to present clear peaks of the dominant frequency on every measurement data. The obtained values are consistent with the literature, regarding the lithology and the geological condition, as described in (Bindi et al., 2011). Location A has dominant frequencies ranging around 2.5 to 5.0 Hz, with the amplification factor of 2.0 to 5.2. Whereas, location B has dominant frequencies ranging from 7.0 to 9.0 Hz, with amplification factor from 2.3 to 4.2. These results verify the sedimentation thickness on the location, which is 32 to 64 meters at location A and 18 to 23 meters at location B. The complexity of the spectral profile implies the complexity of the subsurface structure. We found a smooth HVSR profile from location A, indicating a more homogeneous sedimentary layer on that site. In contrast, the profile obtained from location B is undulating both at lower and higher frequency. This is the indication that the site is having a more complex subsurface structure.

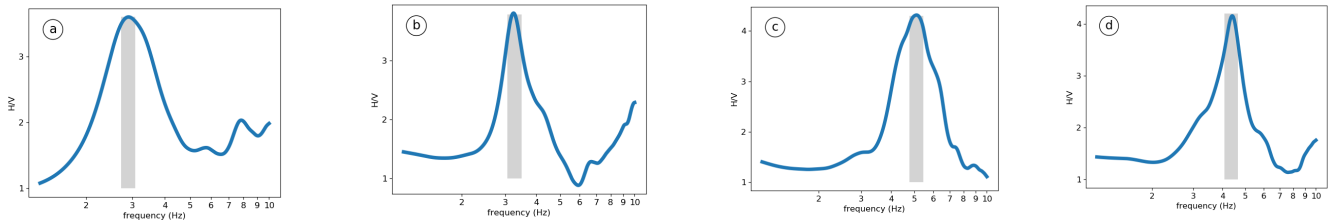

Figure 5. Exemplary HVSR curve from the measurement at location A. The H/V curve of the data in figure 3 is shown in (a). The x-axis indicates dominant frequency (Hz) and y-axis indicates amplification factor (H/V). The peak of the curve shows the value of the dominant frequency and amplification factor. In this figure, the dominant frequency value obtained is 2.9 to 5.0 Hz and the amplification factor is 3.5 to 4.3

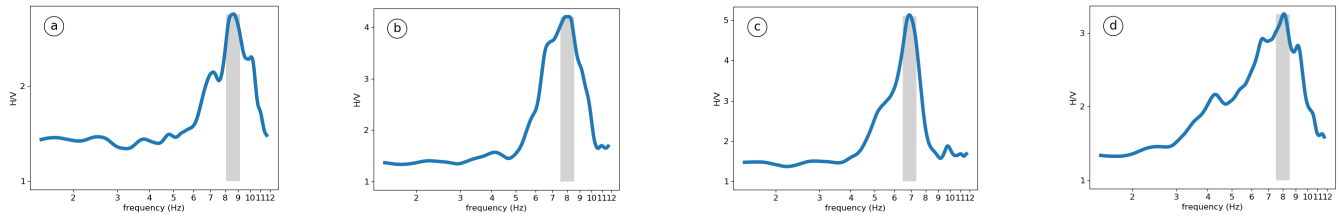

Figure 6. Exemplary HVSR curve from the measurement at location B. The dominant frequency value obtained is 7.0 to 8.5 Hz and the amplification factor is 2.8 to 5.0

Statistical calculations were carried out to measure the fluctuation of the observed frequencies. Figure 7 shows the plot of the standard error calculation for the exemplary data shown in figure 3. The standard error value obtained at the highest peak of the curve (the resonance frequency) is 0.14. This value is fairly small, so the result of our calculation of the HVSR curve is acceptable. From all the acquired data, we can assume that the precision of our measurement is within 1.5 Hz, regarding the maximum standard error of 0.68 Hz. The precision may decrease at the higher frequency dominated area. At the location B, we can only claim 2 Hz of precision from the maximum standard error of 0.89 Hz. Nevertheless, we are convinced that the system that we developed is adequate and able to obtain a correct result in the range of frequencies 2 to 10 Hz.

Data validation was also carried out by comparing the results of sediment thickness obtained based on references. The results of measurements made by PSG in the first area have a sediment thickness value

of 25 to 65 meters. In this work, the sediment thickness values obtained in the first area are in the range of 32 to 64 meters. Meanwhile, the sediment thickness in the second area is 18 to 23 meters, thinner than the first region. Based on these results, the results of our work are in accordance with the literature used. In the range of dominant frequency values obtained, these sediments are alluvial deposits or in the form of soil resulting from weathering of rocks (Kanai, 1983; Telford, 2021). Meanwhile, the value of the amplification factor that represents the vulnerability of the research area when exposed to shocks is in the low to medium category (Kanai, 1983). Thus, this area is included in the safe category for development areas.

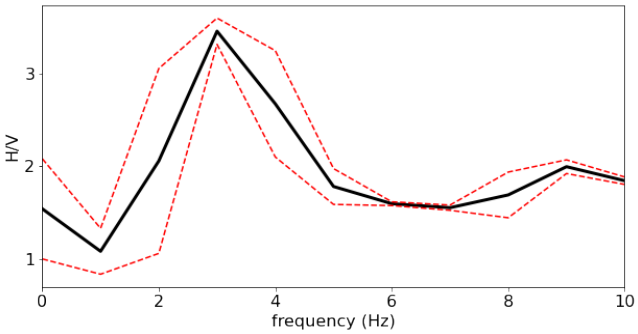

Figure 7. Standard error calculation of the HVSR curve. The red-dashed line indicates standard error value. The highest peak of the curve is the resonance frequency

Table 2. The Result of Dominant Frequencies Calculated by the HVSR Method from the First Location (A). The H/V Column Represents the Amplification Value

Measurement Location	Dominant Frequency (Hz) ± Standard Error	H/V	Sediment Thickness (m)
A1	5.0 ± 0.29	2.0	32
A2	5.0 ± 0.55	5.2	32
A3	4.2 ± 0.31	3.5	38
A4	2.9 ± 0.14	3.8	46
A5	2.5 ± 0.28	2.0	64
A6	4.2 ± 0.67	2.1	38
A7	3.1 ± 0.42	3.5	52
A8	4.1 ± 0.31	4.2	39
A9	2.8 ± 0.54	3.9	58
A10	2.8 ± 0.64	4.0	58
A11	2.5 ± 0.32	5.0	64
A12	2.6 ± 0.12	3.2	62
A13	3.6 ± 0.23	3.8	44
A14	3.5 ± 0.66	2.7	46
A15	4.4 ± 0.11	3.8	36
A16	3.1 ± 0.10	4.0	52
A17	4.3 ± 0.36	4.1	37
A18	4.0 ± 0.55	3.5	40
A19	4.2 ± 0.33	3.2	38
A20	5.0 ± 0.68	4.3	32
A21	4.8 ± 0.22	4.5	33
A22	3.7 ± 0.24	3.7	43
A23	3.2 ± 0.38	3.2	50
A24	4.0 ± 0.61	4.3	40
A25	4.3 ± 0.43	3.5	37
A26	3.9 ± 0.27	3.8	41
A27	5.0 ± 0.23	4.1	32
A28	4.4 ± 0.11	5.0	36
A29	3.8 ± 0.14	2.1	42
A30	4.0 ± 0.55	4.7	40

Table 3. The Result of Dominant Frequencies Calculated by the HVSR Method from the Second Location (B). The H/V Column Represents the Amplification Value

Measurement location	Dominant frequency (Hz) ± standard error	H/V	Sediment thickness (m)
B1	8.7 ± 0.17	2.4	18
B2	7.0 ± 0.08	2.9	23
B3	8.0 ± 0.89	3.2	20
B4	7.8 ± 0.04	3.3	21
B5	8.5 ± 0.08	2.8	19
B6	8.8 ± 0.24	2.3	18
B7	8.5 ± 0.06	2.4	19
B8	8.0 ± 0.43	4.2	20
B9	7.0 ± 0.32	5.0	23
B10	9.0 ± 0.56	3.5	18

The map of the distribution of dominant frequency values in the first location is shown in Figure 8. The data taken on location B is not sufficient to be plotted as a map. It has served the purpose to verify the correctness of the procedure. The map shows an inhomogeneity of the local area, providing detailed information on the subsurface structure variation, which may be important for other fields such as civil engineering, which suggest the frequency that has to be avoided on building an infrastructure. The highest resonance frequency is located in the Northwest part of the measurement site, indicating the shallowest layer of the sediment. In this case 32 meters of sediment thickness. The thickest can be found around the center of site A, of around 64 meters. In figure 8.b we calculated the amplification factor map, derived from the frequency map and the shear velocity of the sedimentation layer and the base layer at every point in the map. The red zones in the map indicate the locations that are more prone to ground shaking, in the case of earthquakes. We found that the dominant frequency and the amplification factor are weakly correlated. This fact originates from a complex relationship between the amplification factor, lithology, and topography of an area. However, the collected data has shown the method is satisfactory in order to reveal the subsurface structure complexity, especially in a volcanic alluvial region where the sedimentation process may bury preexistence structures.

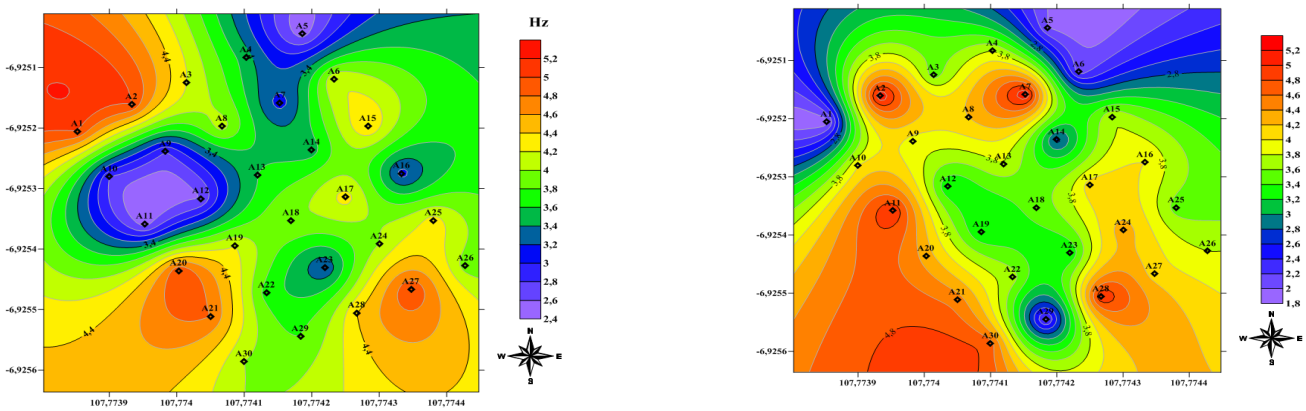

Figure 8. The mapping of (a) the resonance frequency and (b) the amplification factor

Conclusion

The HVSR analysis has been carried out on three-component passive seismic data acquired using an in-house developed seismometer system. This work has shown that the instrument is adequate and able to measure correct physical properties of sediment at the volcanic alluvial lithology. To give a summary, in this work we obtained the correct resonance frequencies which are directly related to the thickness of the sedimentary layer. The result for the thick sediment area is in the range of 32 to 64 meters, consistent with the literature. For the thin sediment area, we obtain a higher resonance frequency, which is 18 to 23 meters, also consistent with the available literature, with acceptable error deviation. The frequencies are in the range of alluvial deposits or in the form of soil resulting from weathering of rocks. We calculated the amplification factor based on the measurement data, and found out that the chosen areas are situated in the low to medium category of disaster vulnerability. As stated previously, the aim of this work is to verify the correctness of measurement and computation procedure, in order to implement the environmental monitoring based on the measurement of ground vibration. The obtained data is very important, in order to predict damage that may be caused by natural disaster and suppress casualties in case of catastrophic events, considering the geological situation of the Bandung Basin. In the future work we intend to build more instrumentation systems to be deployed around the rim of the basin, and perform continuous monitoring of the ground vibration.

Acknowledgements

We are grateful for funding from the Indonesian Collaborative Research (RKI) project, contract no. 2203/UN6.3.1/ PT00/2022. We acknowledge the data support from the Pusat Survei Geology (PSG), Ministry of Energy and Mineral Resources, Republic of Indonesia. EF and YR are thankful for the personal discussions with Marjiyono, M.Sc and Hidayat, M.T.

References

Bao, F., Li, Z., Tian, B., Wang, L., & Tu, G. (2019). Sediment thickness variations of the Tangshan fault zone in North China from a dense seismic array and microtremor survey. *Journal of Asian Earth Sciences*, *185*, 104045.

https://doi.org/10.1016/j.jseaes.2019.104045

Bindi, D., Luzi, L., Parolai, S., Giacomo, D. Di, & Monachesi, G. (2011). Site effects observed in alluvial basins: The case of Norcia (Central Italy). *Bulletin of Earthquake Engineering*, *9*(6), 1941–1959. https://doi.org/10.1007/s10518-011-9273-3

Bonnefoy-Claudet, S., Baize, S., Bonilla, L. F., Berge-Thierry, C., Pasten, C., Campos, J., Volant, P., & Verdugo, R. (2009). Site effect evaluation in the basin of Santiago de Chile using ambient noise measurements. *Geophysical Journal International*, *176*(3), 925–937. https://doi.org/10.1111/j.1365-246X.2008.04020.x

Bowden, D. C., & Tsai, V. C. (2017). Earthquake ground motion amplification for surface waves. *Geophysical Research Letters*, *44*(1), 121–127. https://doi.org/10.1002/2016GL071885

Chemsitra, P., Utama, W., & Syaeful, A. (2018). Identifikasi litologi lapisan sedimen pada daerah karst Pacitan menggunakan metode mikrotremor HVSR. *Jurnal Teknik ITS*, *7*(1), C77–C80. https://doi.org/10.12962/j23373539.v7i1.29370

Di Giacomo, D., Gallipoli, M. R., Mucciarelli, M., Parolai, S., & Richwalski, S. M. (2005). Analysis and modeling of HVSR in the presence of a velocity inversion: The case of Venosa, Italy. *Bulletin of the Seismological Society of America*, *95*(6), 2364–2372. https://doi.org/10.1785/0120040242

Dvorkin, J. P., & Mavko, G. (2006). Modeling attenuation in reservoir and nonreservoir rock. *Leading Edge (Tulsa, OK)*, *25*(2), 194–197. https://doi.org/10.1190/1.2172312

Gosar, A. (2007). Microtremor HVSR study for assessing site effects in the Bovec basin (NW Slovenia) related to 1998 Mw5.6 and 2004 Mw5.2 earthquakes. *Engineering Geology*, *91*(2–4), 178–193. https://doi.org/10.1016/j.enggeo.2007.01.008

Gosar, A. (2017). Study on the applicability of the microtremor HVSR method to support seismic microzonation in the town of Idrija (W Slovenia). *Natural Hazards and Earth System Sciences*, *17*(6), 925–937. https://doi.org/10.5194/nhess-17-925-2017

Herak, M. (2008). ModelHVSR-A Matlab® tool to model horizontal-to-vertical spectral ratio of ambient noise. *Computers and Geosciences*, *34*(11), 1514–1526. https://doi.org/10.1016/j.cageo.2007.07.009

Imposa, S., Lombardo, G., Panzera, F., & Grassi, S. (2018). Ambient vibrations measurements and 1D site response modelling as a tool for soil and building properties investigation. *Geosciences (Switzerland)*, *8*(3), 87. https://doi.org/10.3390/geosciences8030087

Kagawa, T., Noguchi, T., Yoshida, S., & Yamamoto, S. (2017). Effect of the surface geology on strong ground motions due to the 2016 Central Tottori Earthquake, Japan. *Earth, Planets and Space*, *69*(1), 1–8. https://doi.org/10.1186/s40623-017-0689-0

Kaiser, A., Massey, C., & Holden, C. (2014). Site amplification, polarity and topographic effects in the Port Hills during the Canterbury earthquake sequence. *AGU Fall Meeting Abstracts*, *121*, 1–33. https://ui.adsabs.harvard.edu/abs/2014AGUFM.S12A..06K/abstract

Kanai, K. (1983). *Engineering seismology*. University of Tokyo Press.

Landés, M., Hubans, F., Shapiro, N. M., Paul, A., & Campillo, M. (2010). Origin of deep ocean microseisms by using teleseismic body waves. *Journal of Geophysical Research: Solid Earth*, *115*(5). https://doi.org/10.1029/2009JB006918

Marjiyono. (2010). *Estimasi Karakteristik Dinamika Tanah Dari Data Mikrotremor Wilayah Bandung*. Thesis ITB.

Mirzaoglu, M., & Dýkmen, Ü. (2003). Application of microtremors to seismic microzoning procedure. *Journal of the Balkan Geophysical Society*, *6*(3), 143–156. https://www.balkangeophysoc.gr/online-journal/2003_V6/aug2003/Mirzaoglu_final.PDF

Nakamura, Y. (1989). Method for dynamic characteristics estimation of subsurface using microtremor on the ground surface. *Quarterly Report of RTRI (Railway Technical Research Institute) (Japan)*, *30*(1), 25–33. https://trid.trb.org/view/294184

Nogoshi, M., & Igarashi, T. (1971). On the Amplitude Characteristics of Microtremor (Part 2). *Zisin (Journal of the Seismological Society of Japan. 2nd Ser.)*, *24*(1), 26–40. https://doi.org/10.4294/zisin1948.24.1_26

Rezaei, S., & Choobbasti, A. J. (2017). Application of the microtremor measurements to a site effect study. *Earthquake Science*, *30*(3), 157–164. https://doi.org/10.1007/s11589-017-0187-2

Shi, Q., Wu, N., Ma, X., & Wang, H. (2018). Frequency-Domain Joint Channel Estimation and Decoding for Faster-Than-Nyquist Signaling. *IEEE Transactions on Communications*, *66*(2), 781–795. https://doi.org/10.1109/TCOMM.2017.2768063

Stanko, D., Markušić, S., Strelec, S., & Gazdek, M. (2017). HVSR analysis of seismic site effects and soil-structure resonance in Varaždin city (North Croatia). *Soil Dynamics and Earthquake Engineering*, *92*, 666–677. https://doi.org/10.1016/j.soildyn.2016.10.022

Suhendra, Zul Bahrum, C., & Sugianto, N. (2018). Geological condition at landslides potential area based on microtremor survey. *ARPN Journal of Engineering and Applied Sciences*, *13*(8), 3007–3013. https://www.arpnjournals.org/jeas/research_papers/rp_2018/jeas_0418_7026.pdf

Telford, W. ., Geldart, L. ., & Sheriff, R. . (1990). Applied Geophysics. In *Cambridge university press*.

https://doi.org/10.2307/1784540
Telford, W. M. (2021). *Atlas Karakteristik Fisis Sedimen Permukaan Cekungan Bandung* (1st ed.). Pusat Survei Geologi (PSG).